

## On the Distances to the X-ray Binaries Cygnus X-3 and GRS 1915+105

M. J. REID <sup>1</sup> AND J. C. A. MILLER-JONES <sup>2</sup>

<sup>1</sup>*Center for Astrophysics | Harvard & Smithsonian, 60 Garden Street, Cambridge, MA 02138, USA*

<sup>2</sup>*International Centre for Radio Astronomy Research, Curtin University, GPO Box U1987, Perth, WA 6845, Australia*

### ABSTRACT

In this paper we significantly improve estimates of distance to the X-ray binary systems Cyg X-3 and GRS 1915+105. We report a highly accurate trigonometric parallax measurement for Cyg X-3 using the VLBA at 43 GHz, placing the source at a distance of  $9.67_{-0.48}^{+0.53}$  kpc. We also use Galactic proper motions and line-of-sight radial velocity measurements to determine 3-dimensional (3D) kinematic distances to both systems, under the assumption that they have low peculiar velocities. This yields distances of  $8.95 \pm 0.96$  kpc for Cyg X-3 and  $9.4 \pm 0.6$  (statistical)  $\pm 0.8$  (systematic) for GRS 1915+105. The good agreement between parallax and 3D kinematic distances validates the assumption of low peculiar velocities, and hence small natal kicks, for both of the systems. For a source with a low peculiar velocity, given its parallax distance, Cyg X-3 should have a  $V_{\text{LSR}}$  near  $-64 \pm 5$  km s<sup>-1</sup>. Our measurements imply a slightly higher inclination angle, and hence lower black hole mass for GRS 1915+105 than found from previous work by Reid et al. (2014) and strengthen arguments from X-ray polarization that Cyg X-3 would be an ultraluminous X-ray source if viewed face-on.

### 1. INTRODUCTION

Knowledge of the distance to an astronomical source is fundamental for estimating its true nature, including its mass and luminosity. The case of the high-mass X-ray binary Cyg X-1 is an excellent example. It was the first binary suggested to include a black hole, based on its periodic velocity excursions and the lack of an observable companion (Webster & Murdin 1972; Bolton 1972). However, for nearly 40 years, one could not be certain whether the companion was a black hole or a neutron star, since distance estimates ranged by more than a factor of two, from about 1.1 to 2.5 kpc (see, e.g., Caballero-Nieves et al. 2009), and at the lower end of the range of distances companion masses could be below about 5  $M_{\odot}$ . This problem was resolved by Reid et al. (2011) and Miller-Jones et al. (2021), using the Very Long Baseline Array (VLBA) to observe the radio emission from the compact companion and measure a trigonometric parallax relative to background quasars, with the latter study

yielding a distance of  $2.22^{+0.18}_{-0.17}$  kpc. This firmly established that the Cyg X-1 system contains a black hole and a massive young star.

However, accurate parallaxes for more distant X-ray binaries have been hard to obtain. In particular, two well-studied X-ray binaries, GRS 1915+105 and Cyg X-3, have large distance uncertainties, which limit our understanding of their nature. Reid et al. (2014) observed GRS 1915+105 with the VLBA and measured a *relative* parallax to a nearby (in both projection and distance) water maser associated with a massive, young star. Combining the relative parallax of GRS 1915+105 with the absolute parallax of the maser (Wu et al. 2014), and prior constraints on distance based on models of jet kinematics, resulted in a distance estimate for GRS 1915+105 of  $8.6^{+2.0}_{-1.6}$  kpc and led to an estimate of its compact companion mass of  $12.4^{+2.0}_{-1.8} M_{\odot}$ . Previous distance estimates had only indirectly constrained it to be larger than about 6 kpc, inferred from H I absorption (Mirabel & Rodríguez 1994), and smaller than 12.5 kpc, based on the ratio of apparent speeds of the approaching and receding jets (Fender et al. 1999).

Determining the distance to Cyg X-3 has been less successful than for GRS 1915+105. Dickey (1983) noted that there is absorption from interstellar H I toward Cyg X-3 from Local Standard of Rest velocities,  $V_{\text{LSR}}$ , of zero to at least  $-70 \text{ km s}^{-1}$ , suggesting a lower limit for its distance of  $> 11.6 \times (R_0/10 \text{ kpc})$ , where  $R_0$  is the distance to the Galactic center. Predehl et al. (2000) compared the angular extent of the X-ray halo of Cyg X-3 with the time delay of X-rays scattered by intervening dust and estimated a distance of  $9^{+4}_{-2}$  kpc. Ling et al. (2009) re-analyzed the X-ray data and, assuming that the scattering occurs in the Cyg OB2 association of young stars at 1.7 kpc, estimated a distance of Cyg X-3 of  $7.2^{+0.3}_{-0.5}$  kpc. However, allowing the Cyg OB2 distance to be between 1.38 and 1.82 kpc places Cyg X-3 between 3.4 and 9.3 kpc distant.

In this paper we present a very accurate trigonometric parallax for the high-mass X-ray binary Cyg X-3, as well as an independent estimate of its distance using 3-dimensional (3D) kinematics. For the micro-quasar GRS 1915+105, which already has a trigonometric parallax measurement, we also provide an independent estimate of distance using 3D kinematics. Finally, we carefully examine the fundamental assumption of kinematic distances – that the sources have only small to moderate ( $\lesssim 20 \text{ km s}^{-1}$ ) non-circular motions – as this has strong implications for how some compact stars can form, since it requires small natal “kicks.”

## 2. ESTIMATING DISTANCE WITH 3D MOTIONS

Reid (2022) analyzed the use of proper motions in addition to line-of-sight velocities to obtain 3D kinematic distance estimates, concluding that they had great potential for sources more distant than about 8 kpc. 3D kinematic distance estimates compare the full observed velocity vector to a model of Galactic rotation, with distance as an adjustable parameter. The fundamental Galactic parameters – the distance to the Galactic center ( $R_0$ ), the circular rotation speed of the Sun ( $\Theta_0$ ), and the rotation curve of the Milky Way – are now known to near 1% accuracy (see Reid et al. 2019; Do et al. 2019; Reid & Brunthaler 2020; GRAVITY Collaboration et al. 2021, for details). For distant sources, measurements of proper motion

can require orders of magnitude less precision compared to parallax measurements for similar fractional distance uncertainty. Thus, 3D kinematic distances offer an opportunity to refine distance estimates for sources that follow Galactic rotation.

For the Galactic model needed for kinematic distance estimates, we assume the values of  $R_0 = 8.15$  kpc and  $\Theta_0 = 236$  km s<sup>-1</sup> from Reid et al. (2019) and their Solar Motion parameters ( $U_\odot = 10.6, V_\odot = 10.7, W_\odot = 7.6$ ) km s<sup>-1</sup>. For the rotation curve of the Milky Way, we adopt that of Reid et al. (2019, documented in their appendix B). This rotation curve model follows the 2-parameter “universal” formulation of Persic et al. (1996) and was obtained by fitting 147 maser sources with Galactocentric radii between 4 and 15 kpc using measured 3D motions and “gold standard” parallax distances. Following Reid (2022), we estimate 3D kinematic distances by forming likelihoods as a function of distance for three components of motion: the velocity with respect to the Local Standard of Rest,  $V_{\text{LSR}}$ , the proper motion in Galactic longitude,  $\mu_l$ , and the proper motion in Galactic latitude,  $\mu_b$ . Assuming a flat prior on distance, the product of these likelihoods gives the combined posterior distribution function (PDF) for distance.

### 3. GRS 1915+105

The proper motion of GRS 1915+105 has been measured relative to compact extra-galactic sources by Dhawan et al. (2007) and Reid et al. (2014) using the VLBA of the National Radio Astronomy Observatory<sup>1</sup>. Dhawan et al. (2007) observed predominantly at 8.4 GHz between 1996 and 2006 and achieved single-epoch astrometric precision of  $\approx 1$  mas. They measured the eastward and northward motions to be  $\mu_\alpha = -2.86 \pm 0.07$  mas y<sup>-1</sup> and  $\mu_\delta = -6.20 \pm 0.09$  mas y<sup>-1</sup>. Independently, Reid et al. (2014) observed at 22 GHz between 2008 and 2013 and with improved astrometric techniques, including using “geodetic blocks” to measure and remove residual tropospheric delays (Reid et al. 2009), and achieved single-epoch precision of  $\approx 0.2$  mas, yielding  $\mu_\alpha = -3.19 \pm 0.03$  mas y<sup>-1</sup> and  $\mu_\delta = -6.24 \pm 0.05$  mas y<sup>-1</sup>. The variance-weighted average is  $\mu_\alpha = -3.14 \pm 0.03$  mas y<sup>-1</sup>,  $\mu_\delta = -6.23 \pm 0.04$  mas y<sup>-1</sup>, which converts to motions in Galactic longitude and latitude of  $\mu_l = -6.98 \pm 0.05$  mas y<sup>-1</sup>,  $\mu_b = -0.12 \pm 0.01$  mas y<sup>-1</sup>. Reid et al. (2014) recalibrated the data of Steeghs et al. (2013) and estimated the heliocentric line-of-sight velocity  $\gamma = +12.3 \pm 1.0$  km s<sup>-1</sup>, corresponding to a  $V_{\text{LSR}} = 30.4$  km s<sup>-1</sup>.

Figure 1 displays the likelihood functions for the three components of motion of GRS 1915+105. The line-of-sight velocity ( $V_{\text{LSR}}$ ) gives maximum likelihood distances of 1.80 or 9.65 kpc; the Galactic longitude proper motion favors a distance of 8.15 kpc; and the latitude motion weakly constrains the distance (favoring a large value). The combined 3D kinematic distance estimate for GRS 1915+105 is  $9.4 \pm 0.6$  (statistical)  $\pm 0.8$  (systematic) kpc, where the statistical uncertainty is a Gaussian  $1\sigma$  width of the combined PDF and the systematic uncertainty is half of the separation of the peaks of the line-of-sight ( $V_{\text{LSR}}$ ) and longitude motion ( $\mu_l$ ) likelihoods.

<sup>1</sup> The National Radio Astronomy Observatory is a facility of the National Science Foundation operated under cooperative agreement by Associated Universities, Inc.

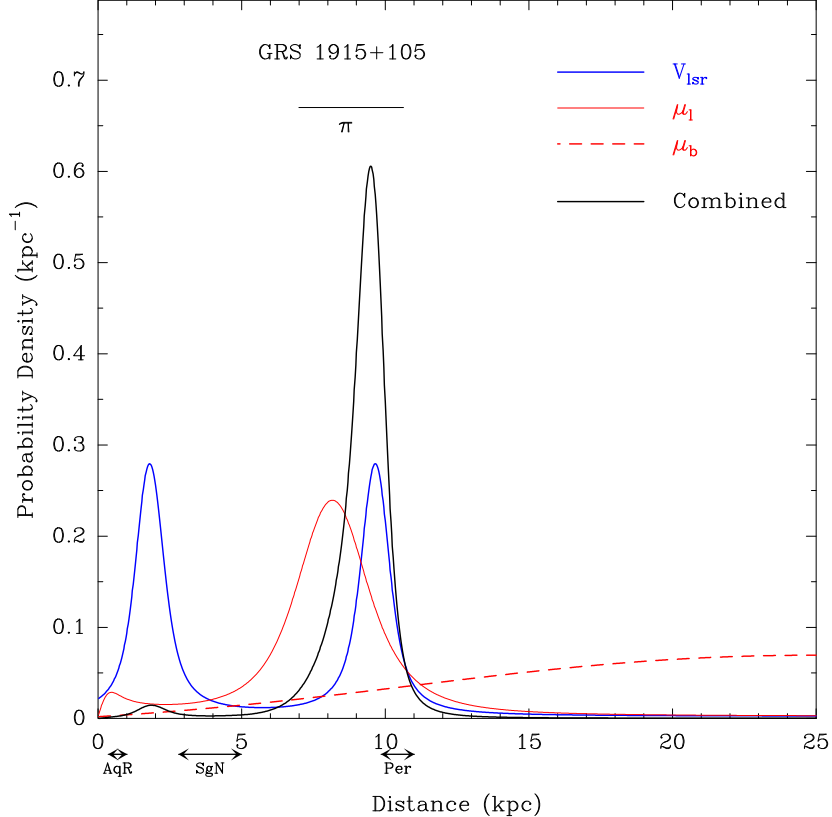


**Figure 1.** Likelihoods for three components of motion,  $V_{\text{LSR}}$  in (*blue*), Galactic longitude (*red solid line*) and latitude (*red dashed line*), as a function of distance for GRS 1915+105. The product of the three likelihoods is shown in *black*, indicating a distance of  $9.4 \pm 0.6$  (statistical)  $\pm 0.8$  (systematic) kpc. The parallax-based distance from Reid et al. (2014) is indicated with the  $\pi$  symbol and its 68% confidence range is given above it. The range of distances for spiral arms along the line-of-sight are indicated below the distance axis.

Using the same fundamental parameters of the Milky Way adopted for the model for the 3D kinematic distance, the non-circular (peculiar) motion components for GRS 1915+105 are  $(U, V, W) = (18 \pm 2, 8 \pm 22, 2 \pm 2)$  km s<sup>-1</sup>, where  $U$  is toward the Galactic center,  $V$  is in the direction of Galactic rotation, and  $W$  is toward the North Galactic Pole. Thus, the magnitude of the peculiar motion of GRS 1915+105 is fairly small ( $\sim 20$  km s<sup>-1</sup>).

## 4. CYG X-3

### 4.1. Trigonometric Parallax

Previous attempts to measure the parallax of Cyg X-3 used the VLBA under program BM343. Those observations at 12 GHz employed background quasars for calibration which were separated from Cyg X-3 by  $\approx 3^\circ$ . Owing to this large separation, these observations yielded only a marginal parallax detection. The lack of compact quasars near Cyg X-3 is a result of strong scattering from interstellar electrons over a few degrees on the sky toward the Cygnus X region. Such scattering increases the apparent angular size of radio sources, making them heavily resolved on long interferometer baselines. Since scattering angles decrease as the inverse-square of observing frequency, in order to minimize scatter broadening and find a

closer background source, we surveyed continuum radio sources within  $2^\circ$  of Cyg X-3 with the VLBA at 43 GHz and found one, J2033+4000, which was relatively compact and separated by only  $1^\circ$  from Cyg X-3.

In VLBA program BR212, we observed Cyg X-3 and J2033+4000 at 43 GHz at eight epochs spanning one year. The calibrator, J2033+4000, was resolved on the longest baselines, and we only used seven antennas (stations codes: BR, FD, KP, LA, NL, OV, PT) with a maximum baseline length of 2300 km. We “nodded” the array between the two sources, changing sources every 20 sec, in order to transfer phase from J2033+4000 to Cyg X-3 within the interferometer coherence time, limited by rapid fluctuations in water vapor. We also calibrated the slowly varying (hours time-scale) changes in total water vapor above each antenna by observing “geodetic-like” blocks of quasars at 24 GHz across the sky. These and other calibration methods are described in detail in Reid et al. (2009). The data were correlated using the VLBA DiFX software correlator (Deller et al. 2011), and analyzed using the Astronomical Image Processing System (Greisen 2003).

Fig. 2 shows a representative image of Cyg X-3 from observations on 2017 May 14. The northern bright spot was clearly visible at all epochs and served as the astrometric point for the parallax measurement. Table 1 gives the dates of the observation, and measured positions and brightnesses for Cyg X-3 obtained by fitting a Gaussian brightness distribution to the northern spot.

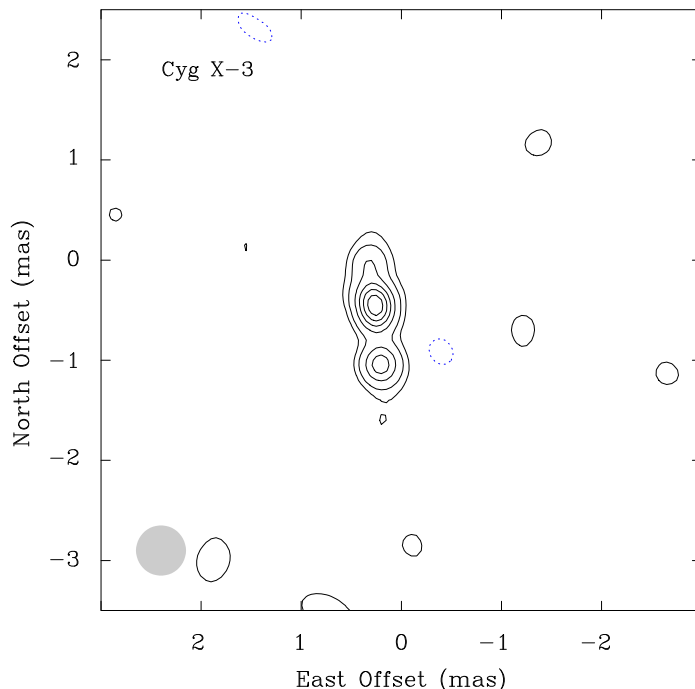


**Figure 2.** VLBA contour map of Cyg X-3 at 43 GHz on 2017 May 14 when the source was weakest. Contour levels are -0.5, 0.5, 1.0, 2.0, 3.0, 4.0, 5.0 mJy. A 0.5 mas FWHM beam is shown as the shaded disk at the bottom left. The brightest component, near (0.2, -0.5) mas, was used for fitting the parallax.

**Table 1.** Parallax Data for Cyg X-3

Date	East Offset (mas)	North Offset (mas)	Brightness (mJy beam <sup>-1</sup> )
2016.806	1.495 ± 0.003	1.702 ± 0.005	18.5 ± 0.2
2016.836	1.425 ± 0.004	1.548 ± 0.007	19.0 ± 0.4
2017.308	0.397 ± 0.001	-0.072 ± 0.002	40.2 ± 0.3
2017.325	0.346 ± 0.006	-0.159 ± 0.007	15.3 ± 0.4
2017.344	0.291 ± 0.004	-0.319 ± 0.005	13.6 ± 0.2
2017.368	0.266 ± 0.007	-0.441 ± 0.010	6.7 ± 0.2
2017.815	-1.126 ± 0.003	-2.146 ± 0.004	16.8 ± 0.2
2017.847	-1.185 ± 0.005	-2.180 ± 0.007	14.2 ± 0.4

NOTE—Column 1 gives the date of the observation. Columns 2 and 3 give the measured position offsets of Cyg X-3 relative to J2033+4000, after removing a constant angular difference assuming J2000 coordinates of (20:32:25.76955,+40:57:27.8820) for Cyg X-3 and (20:33:03.671208,+40:00:24.40818) for J2033+4000. Column 4 gives the peak brightness obtained for Cyg X-3 by fitting a Gaussian distribution. Typical beam sizes were 0.5 mas FWHM. All errors are formal  $1\sigma$  fitting uncertainties and do not include systematic errors.

The relative positions in Table 1 were modeled by a trigonometric parallax signature and a linear proper motion and fitted by variance-weighted least squares. In order to account for delay errors from uncompensated tropospheric water vapor, we added “error floors” in quadrature to the formal uncertainties in the East and North offsets. The error floors were adjusted to  $(\sigma_E, \sigma_N) = (\pm 0.014, \pm 0.070)$  mas to give a reduced chi-squared per degree of freedom near unity in each coordinate. The reason for the error floor in the northerly direction,  $\sigma_N$ , being five-times larger than in the easterly direction,  $\sigma_E$ , is likely due to unresolved jitter in the core position owing to weak jetted emission in the North-South direction.

Fig. 3 displays the parallax data and fits, as sky positions for all epochs, as well as East and North offsets as a function of time. The best-fit parallax is  $0.1034 \pm 0.0054$  mas. With just a 5% uncertainty, we can simply invert the parallax to determine the distance, without the need for a prior. This gives a distance of  $9.67_{-0.48}^{+0.53}$  kpc. The eastward and northward components of proper motion are  $-2.589 \pm 0.014$  and  $-3.747 \pm 0.069$  mas  $y^{-1}$ .

#### 4.2. 3D Kinematic Distance

The proper motion of Cyg X-3 had been measured relative to compact extragalactic sources by Miller-Jones et al. (2009) to be  $\mu_\alpha = -2.73 \pm 0.06$  mas  $y^{-1}$  and  $\mu_\delta = -3.70 \pm 0.06$  mas  $y^{-1}$  using mostly Very Large Array A-configuration observations spanning 1983 to 2006 at 8.4

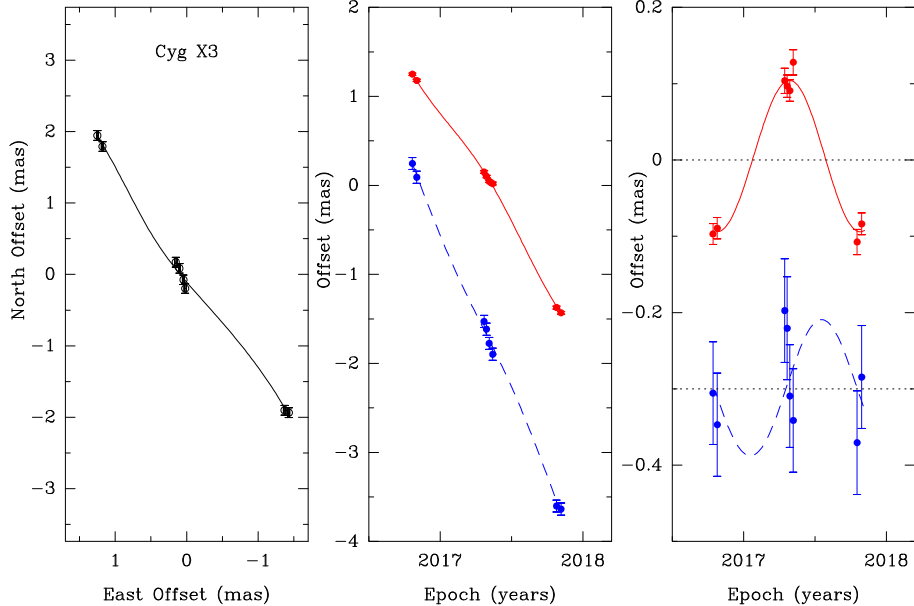


**Figure 3.** Parallax data and fits for Cyg X-3. *Left Panel:* Sky view with East and North offsets. *Middle Panel:* East (data and fitted solid line in red) and North (data and fitted dashed line in blue) positions vs. time. *Right Panel:* Same as middle panel, but with fitted proper motion removed to highlight the parallax effect. One-sigma error bars include systematic uncertainty added in quadrature with the formal fitting uncertainties, yielding chi-squared per degree of freedom near unity in each coordinate.

GHz (or higher frequencies). This motion is in reasonable agreement with our more accurate measurement given above.

The line-of-sight velocity of this binary is very poorly constrained, owing to a combination of high visual extinction and the infrared emission lines arising from differing locations in the turbulent wind of the Wolf-Rayet primary, which cannot therefore be used to determine the radial velocity of the system itself (e.g. Koljonen & Maccarone 2017). Here we adopt a very loose prior on  $V_{\text{LSR}}$  of  $-50 \pm 50 \text{ km s}^{-1}$ , which is essentially consistent with it being a Galactic source toward a longitude of  $\approx 80^\circ$ .

Fig. 4 displays the likelihood functions for the three components of motion of Cyg X-3. While the likelihood for its  $V_{\text{LSR}}$  provides no useful constraint on distance, the proper motion component in Galactic longitude strongly (and the latitude component weakly) constrains distance to be  $8.95 \pm 0.96 \text{ kpc}$ . Since the Cyg X-3 binary contains a Wolf-Rayet star, which lives  $\lesssim 10 \text{ Myr}$ , it should be very near its birth location inside a spiral arm of the Milky Way. Fig. 5 shows the latest model of the spiral arms of the Milky Way by Reid et al. (2019), which is based on parallax measurements of  $\approx 150$  massive, young stars. The parallax (and kinematic) distance of Cyg X-3 places it in the Outer spiral arm, which has a Galactic latitude of  $1.7^\circ$  near the  $79.85^\circ$  longitude of Cyg X-3. The latitude of Cyg X-3 differs from that of other Outer arm by about  $1^\circ$ , corresponding to about  $170 \text{ pc}$  at  $9.67 \text{ kpc}$  distance, which is well within the (Gaussian  $1\sigma$ ) vertical width of that arm of about  $200 \text{ pc}$  (extrapolated from figure 4 of Reid et al. 2019).



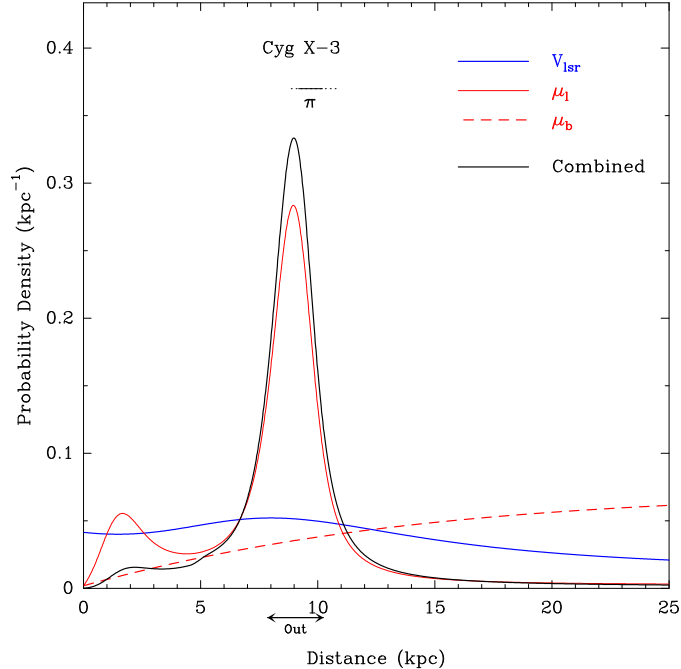


**Figure 4.** Likelihoods for three components of motion,  $V_{\text{LSR}}$  in (*blue*), Galactic longitude (*red solid line*) and latitude (*red dashed line*), as a function of distance for Cyg X-3. The product of the three likelihoods is shown in *black*, indicating a distance of  $8.95 \pm 0.96$  kpc. The parallax distance reported in this paper is indicated with the  $\pi$  symbol, and its 68% and 95% confidence ranges are indicated with *solid* and *dotted* lines above it. The distance range for the Outer spiral arm along the line-of-sight is indicated below the distance axis.

While Cyg X-3 does not have a reliable line-of-sight velocity, its proper motion has been accurately measured and can be compared to those of four massive, young stars with maser astrometry that straddle Cyg X-3 in Galactic longitude and are known to be in the Outer spiral arm, whose locations are shown in Fig. 5. Fig. 6 shows the easterly and northerly proper motions of these stars. Note that both components of motion for Cyg X-3 are consistent with interpolations between the sources, which bracket Cyg X-3 in Galactic longitude. This further supports the association of Cyg X-3 with the Outer arm.

Given the strong evidence that Cyg X-3 formed recently in the Outer spiral arm of the Milky Way, we now examine evidence that can constrain its  $V_{\text{LSR}}$ . The four massive, young stars which straddle Cyg X-3 and have consistent proper motions, have line-of-sight velocities that range from  $-82 < V_{\text{LSR}} < -58$  km s $^{-1}$ . We now calculate the peculiar motion of Cyg X-3 as a function of its (unknown) line-of-sight velocity and display this in Fig. 7. The magnitude of the peculiar motion is less than 20 km s $^{-1}$  for  $-82 < V_{\text{LSR}} < -47$  km s $^{-1}$ , similar to the range of  $V_{\text{LSR}}$  for the four young stars, and there is a clear minimum for the 3D peculiar motion of Cyg X-3 near  $V_{\text{LSR}} = -64$  km s $^{-1}$ . Note that our parallax distance and uncertainty, would yield standard (1D) kinematic distance for  $V_{\text{LSR}} = -64 \pm 5$  km s $^{-1}$ .

All together there is strong circumstantial evidence that Cyg X-3 has a small peculiar motion ( $\lesssim 20$  km s $^{-1}$ ), suggesting a small natal kick when its compact star formed. Indeed, the small value ( $< 1$  km s $^{-1}$ ) of the peculiar motion component toward the North Galactic



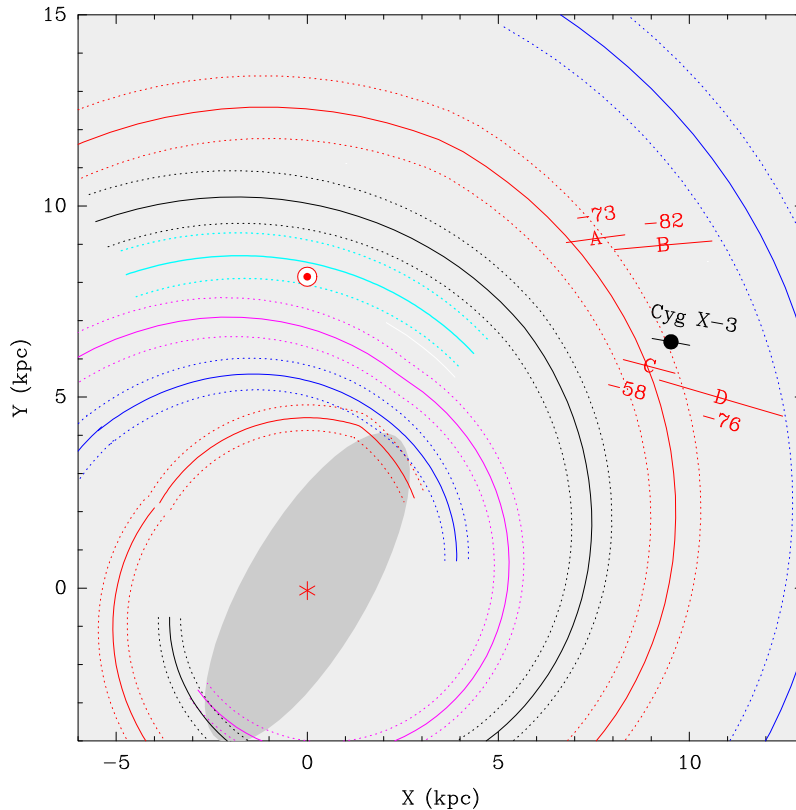


**Figure 5.** Plan-view model of the Milky Way after Reid et al. (2019), indicating the locations of Cyg X-3 (*black dot*) and four massive, young stars with water masers (*red letters*) associated with the Outer spiral arm (*red lines*) between Galactic longitudes  $70^\circ$  and  $100^\circ$  and with parallax distances from VLBI astrometry. A is G097.53+3.18 (Hachisuka et al. 2015; Reid et al. 2019), B is G095.05+3.97 (Sakai et al. 2020), C is G075.30+1.32 (Sanna et al. 2012), and D is G073.65+0.19 (Reid et al. 2019).  $V_{\text{LSR}}$  values in  $\text{km s}^{-1}$  for the masers are indicated next to their positions; each is uncertain by about  $\pm 10 \text{ km s}^{-1}$ .

Pole, which is nearly independent of the  $V_{\text{LSR}}$  of Cyg X-3, supports this conclusion, since it is *a priori* unlikely for a natal kick to be entirely in the Galactic plane.

## 5. DISCUSSION

### 5.1. GRS 1915+105

The 3D kinematic distance estimate for GRS 1915+105 is consistent with, but more precise than, the parallax distance determined by Reid et al. (2014). As noted in that work, the distance affects the inferred black hole mass through its effect on the inclination of the orbit (assumed to be aligned with the jets). The proper motions  $\mu_{\text{app}}$  and  $\mu_{\text{rec}}$  of intrinsically symmetric approaching and receding jet ejecta can be used to constrain the product  $\beta \cos i$ , where  $\beta$  is the jet speed normalized to the speed of light, and  $i$  is the inclination angle of the jet axis to the line of sight. With an accurate distance, these two parameters can be disentangled via

$$\tan i = \frac{2d}{c} \frac{\mu_{\text{app}}\mu_{\text{rec}}}{\mu_{\text{app}} - \mu_{\text{rec}}}. \quad (1)$$

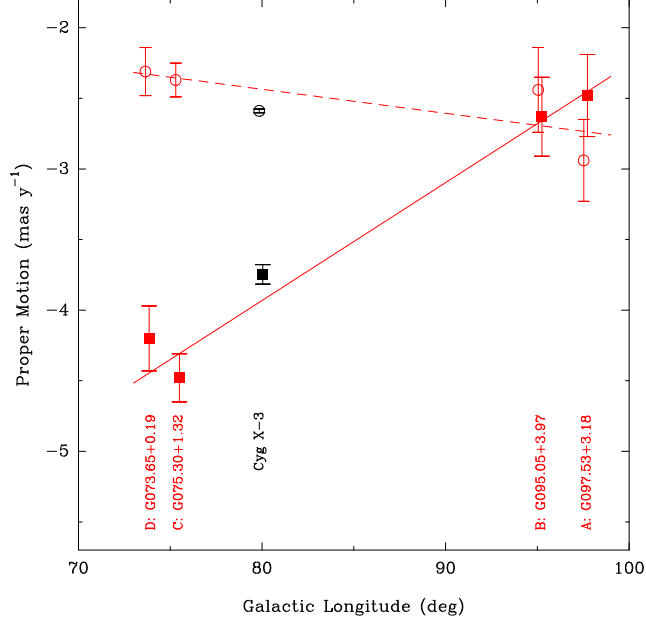


**Figure 6.** Proper motions of four massive, young stars with water masers (*red symbols*) and Cyg X-3 (*black symbols*) as a function of Galactic longitude. Source names are given below their measurements along with letter codes used in Fig. 5 (Sanna et al. 2012; Hachisuka et al. 2015; Reid et al. 2019; Sakai et al. 2020). *Open circles* indicate motions in the easterly direction and *filled squares* indicate motions in the northerly direction. The young stars, which are associated with the Outer spiral arm of the Milky Way and straddle Cyg X-3 in Galactic longitude, have motions consistent with that of Cyg X-3.

The larger distance of GRS 1915+105 inferred from its 3D kinematics implies a larger inclination angle for the jet axis. Using a census of paired ejecta with accurate proper motion measurements from Miller-Jones et al. (2007), we find a weighted mean inclination angle of  $64^\circ \pm 4^\circ$ . The increase in the inferred inclination angle implies a higher jet speed for a given set of proper motion measurements, with the proper motions of Miller-Jones et al. (2007) giving jet speeds ranging from 0.68–0.91 $c$ .

Given the  $\sin^3 i$  dependence of the mass function on inclination, our higher inclination (relative to the  $60^\circ \pm 5^\circ$  determined from the parallax distance estimate by Reid et al. 2014) would translate to a slight reduction in the inferred black hole mass, from  $12.4 M_\odot$  to  $11.2 M_\odot$ . This reduction in inferred black hole mass makes GRS 1915+105 less of an outlier relative to the black hole mass distribution of the low-mass X-ray binary population, as estimated by Farr et al. (2011) and Kreidberg et al. (2012).

As shown by Dhawan et al. (2007), the peculiar velocity of GRS 1915+105 is minimized at distances of between 8 and 10 kpc, such that our 3D kinematic distance does not significantly impact the calculated non-circular motion of the system. At only 36 pc from the Galactic plane, and with a peculiar velocity of  $\sim 20 \text{ km s}^{-1}$ , GRS 1915+105 is likely to have formed either via direct collapse, or in a supernova with a very low natal kick. Indeed, determining the potential kick velocity via the method of Atri et al. (2019), we find a median of  $32 \text{ km s}^{-1}$ ,

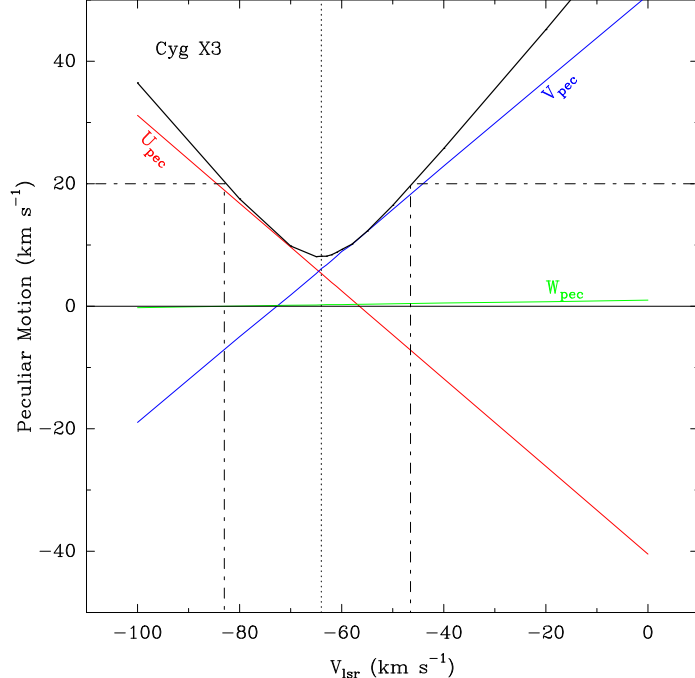


**Figure 7.** Peculiar (non-circular) components of motion of Cyg X-3 as a function of its (unknown) line-of-sight velocity component ( $V_{\text{LSR}}$ ):  $U_{\text{pec}}$  toward the Galactic center (*red*),  $V_{\text{pec}}$  in the direction of Galactic rotation (*blue*), and  $W_{\text{pec}}$  toward the North Galactic Pole (*green*). The 3D magnitude of the peculiar motion is plotted in *black* and has a minimum of  $8 \text{ km s}^{-1}$  at  $V_{\text{LSR}} = -64 \text{ km s}^{-1}$ . The  $V_{\text{LSR}}$  range for the motion magnitude being  $> 20 \text{ km s}^{-1}$  is shown by *dot-dashed lines*. Our parallax distance of  $9.67 \text{ kpc}$  is assumed.

with a 90% confidence interval of  $17\text{--}65 \text{ km s}^{-1}$ . This is comparable to the lowest inferred natal kicks of any low-mass X-ray binary.

## 5.2. *Cyg X-3*

Under the reasonable assumption (supported by strong circumstantial evidence, as detailed in Section 4.2) that the peculiar velocity of Cyg X-3 is small, we determine a 3D kinematic distance of  $8.95 \pm 0.96 \text{ kpc}$ , in good agreement with the independently-determined trigonometric parallax measurement of  $9.67^{+0.53}_{-0.48} \text{ kpc}$ . This provides confidence in the distance determination and validates the effectiveness of the 3D kinematic distance method (Reid 2022) for sources with a low peculiar velocity.

While early distance estimates for Cyg X-3 (Dickey 1983; Predehl et al. 2000) placed the source at a distance of  $\sim 10 \text{ kpc}$ , more recent dust scattering measurements by Ling et al. (2009) favored a lower distance of  $7.2^{+0.3}_{-0.5} \text{ kpc}$ . However, as noted by the authors, this measurement was highly sensitive to the distance of the Cyg OB2 association (assumed as  $1.7 \text{ kpc}$ ), and more recent *Gaia* data (Berlanas et al. 2019) have shown the cluster to be slightly more distant, at  $\sim 1.76 \text{ kpc}$ . Extended X-ray emission which varied on the orbital period of Cyg X-3 was found to arise from X-ray scattering by a Bok globule along the line of sight (McCullough et al. 2013). Standard 1D kinematic distances to the globule with  $V_{\text{LSR}} = -47.5 \text{ km s}^{-1}$  are either  $6.1 \pm 0.6$  or  $7.8 \pm 0.6 \text{ kpc}$ . Modeling the time delay of the scattered light

curve yielded possible distances to Cyg X-3 of either  $7.4 \pm 1.1$  and  $10.2 \pm 1.2$  kpc, at 62 and 38% probability, respectively (McCollough et al. 2016). The farther distance estimate would be fully consistent with our measurement.

Since our distance measurement is consistent with that of earlier works (Dickey 1983; Predehl et al. 2000), the update does not significantly change jet velocities calculated by Mioduszewski et al. (2001) or Miller-Jones et al. (2004). However, Koljonen & Maccarone (2017) noted that a distance of  $\sim 10$  kpc would imply a slight increase in the inferred mass of the Wolf-Rayet donor, to a range of 11–14  $M_{\odot}$ .

Recent X-ray polarization measurements from the Imaging X-ray Polarimetry Explorer (IXPE) suggested that the central compact object in Cyg X-3 is highly obscured (Veledina et al. 2023), likely due to an optically-thick envelope which surrounds a narrow funnel, whose walls allow reflected and scattered light to escape. Unless the opening angle of the funnel was very small ( $\lesssim 16^{\circ}$ ), the inferred geometry would suggest an intrinsic luminosity exceeding the Eddington limit, even for an accretor in excess of  $20M_{\odot}$ . Since these calculations were based on the lower distance of Ling et al. (2009), these inclination angle limits should be even more stringent, strengthening the argument that Cyg X-3 would be an ultraluminous X-ray source if observed face-on.

Furthermore, recent work by Koljonen et al. (2023) suggested a spatial and temporal association between gamma-ray flaring in Cyg X-3 and IceCube neutrino detections, raising the possibility that protons could be accelerated to highly-relativistic energies within the jets of this system, and making Cyg X-3 a possible source of cosmic rays. Our new distance determination would allow for a more accurate assessment of the proton luminosity, and hence the potential cosmic ray contribution of microquasar systems.

## 6. CONCLUSIONS AND OUTLOOK

X-ray binary distance measurements are crucial to understanding their nature, allowing us to determine their underlying physical parameters. For Cyg X-3, we have measured a highly accurate trigonometric parallax distance of  $9.67^{+0.53}_{-0.48}$  kpc. To date, this is the most distant X-ray binary with a radio parallax measurement, demonstrating the potential of VLBI measured parallaxes for bright sources, even at large distances along highly scatter-broadened lines-of-sight. Our refined distance measurement strengthens the argument that Cyg X-3 would appear as an ultraluminous X-ray source if viewed face-on.

Using Cyg X-3’s measured proper motion, we determine a 3D kinematic distance of  $8.95 \pm 0.96$  kpc, which is consistent with the more accurate parallax distance, demonstrating that 3D kinematics can provide reliable distance estimates for X-ray binaries with low peculiar velocities. Both the parallax and kinematic distance locate the system within the Outer spiral arm of the Galaxy. Its proper motion is consistent with those of young, massive stars in the same region, which have LSR velocities near  $-70 \text{ km s}^{-1}$ , suggesting that Cyg X-3 has a similar LSR velocity and supporting a small peculiar velocity of  $< 20 \text{ km s}^{-1}$ .

We also estimated a 3D kinematic distance for GRS 1915+105 of  $9.4 \pm 0.6$  (stat.)  $\pm 0.8$  (sys.) kpc. This distance is consistent with, but more precise than the previous par-

allax result of Reid et al. (2014). At 9.4 kpc, GRS 1915+105 would have a slightly higher inclination angle, and hence lower black hole mass, than previously suggested.

This work underscores the importance of high-precision astrometric measurements of X-ray binary systems, even in cases where a parallax distance measurement is not possible (e.g., due to the lack of a close calibrator, a large distance, or significant scatter broadening). When coupled with a line-of-sight radial velocity measurement, they can provide reliable 3D kinematic distances for sources with low peculiar velocities.

- 1 We thank Arash Bahramian for useful discussions and assistance with fitting jet parameters.
- 2 This work made use of the Swinburne University of Technology software correlator, developed
- 3 as part of the Australian Major National Research Facilities Programme and operated under
- 4 licence. This work has made use of NASA’s Astrophysics Data System.

*Facilities:* VLBA

*Software:* AIPS (Greisen 2003)

## REFERENCES

- Atri, P., Miller-Jones, J. C. A., Bahramian, A., et al. 2019, MNRAS, 489, 3116, doi: [10.1093/mnras/stz2335](https://doi.org/10.1093/mnras/stz2335)
- Berlanas, S. R., Wright, N. J., Herrero, A., Drew, J. E., & Lennon, D. J. 2019, MNRAS, 484, 1838, doi: [10.1093/mnras/stz117](https://doi.org/10.1093/mnras/stz117)
- Bolton, C. T. 1972, Nature, 235, 271, doi: [10.1038/235271b0](https://doi.org/10.1038/235271b0)
- Caballero-Nieves, S. M., Gies, D. R., Bolton, C. T., et al. 2009, ApJ, 701, 1895, doi: [10.1088/0004-637X/701/2/1895](https://doi.org/10.1088/0004-637X/701/2/1895)
- Deller, A. T., Brisken, W. F., Phillips, C. J., et al. 2011, PASP, 123, 275, doi: [10.1086/658907](https://doi.org/10.1086/658907)
- Dhawan, V., Mirabel, I. F., Ribó, M., & Rodrigues, I. 2007, ApJ, 668, 430, doi: [10.1086/520111](https://doi.org/10.1086/520111)
- Dickey, J. M. 1983, ApJL, 273, L71, doi: [10.1086/184132](https://doi.org/10.1086/184132)
- Do, T., Hees, A., Ghez, A., et al. 2019, Science, 365, 664, doi: [10.1126/science.aav8137](https://doi.org/10.1126/science.aav8137)
- Farr, W. M., Sravan, N., Cantrell, A., et al. 2011, ApJ, 741, 103, doi: [10.1088/0004-637X/741/2/103](https://doi.org/10.1088/0004-637X/741/2/103)
- Fender, R. P., Garrington, S. T., McKay, D. J., et al. 1999, MNRAS, 304, 865, doi: [10.1046/j.1365-8711.1999.02364.x](https://doi.org/10.1046/j.1365-8711.1999.02364.x)
- GRAVITY Collaboration, Abuter, R., Amorim, A., et al. 2021, A&A, 647, A59, doi: [10.1051/0004-6361/202040208](https://doi.org/10.1051/0004-6361/202040208)
- Greisen, E. W. 2003, in Astrophysics and Space Science Library, Vol. 285, Information Handling in Astronomy - Historical Vistas, ed. A. Heck, 109, doi: [10.1007/0-306-48080-8\\_7](https://doi.org/10.1007/0-306-48080-8_7)
- Hachisuka, K., Choi, Y. K., Reid, M. J., et al. 2015, ApJ, 800, 2, doi: [10.1088/0004-637X/800/1/2](https://doi.org/10.1088/0004-637X/800/1/2)
- Koljonen, K. I. I., & Maccarone, T. J. 2017, MNRAS, 472, 2181, doi: [10.1093/mnras/stx2106](https://doi.org/10.1093/mnras/stx2106)
- Koljonen, K. I. I., Satalecka, K., Lindfors, E. J., & Liodakis, I. 2023, MNRAS, doi: [10.1093/mnras/slad081](https://doi.org/10.1093/mnras/slad081)
- Kreidberg, L., Bailyn, C. D., Farr, W. M., & Kalogera, V. 2012, ApJ, 757, 36, doi: [10.1088/0004-637X/757/1/36](https://doi.org/10.1088/0004-637X/757/1/36)
- Ling, Z., Zhang, S. N., & Tang, S. 2009, ApJ, 695, 1111, doi: [10.1088/0004-637X/695/2/1111](https://doi.org/10.1088/0004-637X/695/2/1111)

- McCollough, M. L., Corrales, L., & Dunham, M. M. 2016, *ApJL*, 830, L36, doi: [10.3847/2041-8205/830/2/L36](https://doi.org/10.3847/2041-8205/830/2/L36)
- McCollough, M. L., Smith, R. K., & Valencic, L. A. 2013, *ApJ*, 762, 2, doi: [10.1088/0004-637X/762/1/2](https://doi.org/10.1088/0004-637X/762/1/2)
- Miller-Jones, J. C. A., Blundell, K. M., Rupen, M. P., et al. 2004, *ApJ*, 600, 368, doi: [10.1086/379706](https://doi.org/10.1086/379706)
- Miller-Jones, J. C. A., Rupen, M. P., Fender, R. P., et al. 2007, *MNRAS*, 375, 1087, doi: [10.1111/j.1365-2966.2007.11381.x](https://doi.org/10.1111/j.1365-2966.2007.11381.x)
- Miller-Jones, J. C. A., Sakari, C. M., Dhawan, V., et al. 2009, in 8th International e-VLBI Workshop, 17. <https://arxiv.org/abs/0909.2589>
- Miller-Jones, J. C. A., Bahramian, A., Orosz, J. A., et al. 2021, *Science*, 371, 1046, doi: [10.1126/science.abb3363](https://doi.org/10.1126/science.abb3363)
- Mioduszewski, A. J., Rupen, M. P., Hjellming, R. M., Pooley, G. G., & Waltman, E. B. 2001, *ApJ*, 553, 766, doi: [10.1086/320965](https://doi.org/10.1086/320965)
- Mirabel, I. F., & Rodríguez, L. F. 1994, *Nature*, 371, 46, doi: [10.1038/371046a0](https://doi.org/10.1038/371046a0)
- Persic, M., Salucci, P., & Stel, F. 1996, *MNRAS*, 281, 27, doi: [10.1093/mnras/278.1.27](https://doi.org/10.1093/mnras/278.1.27)
- Predehl, P., Burwitz, V., Paerels, F., & Trümper, J. 2000, *A&A*, 357, L25
- Reid, M. J. 2022, *AJ*, 164, 133, doi: [10.3847/1538-3881/ac80bb](https://doi.org/10.3847/1538-3881/ac80bb)
- Reid, M. J., & Brunthaler, A. 2020, *ApJ*, 892, 39, doi: [10.3847/1538-4357/ab76cd](https://doi.org/10.3847/1538-4357/ab76cd)
- Reid, M. J., McClintock, J. E., Narayan, R., et al. 2011, *ApJ*, 742, 83, doi: [10.1088/0004-637X/742/2/83](https://doi.org/10.1088/0004-637X/742/2/83)
- Reid, M. J., McClintock, J. E., Steiner, J. F., et al. 2014, *ApJ*, 796, 2, doi: [10.1088/0004-637X/796/1/2](https://doi.org/10.1088/0004-637X/796/1/2)
- Reid, M. J., Menten, K. M., Brunthaler, A., et al. 2009, *ApJ*, 693, 397, doi: [10.1088/0004-637X/693/1/397](https://doi.org/10.1088/0004-637X/693/1/397)
- . 2019, *ApJ*, 885, 131, doi: [10.3847/1538-4357/ab4a11](https://doi.org/10.3847/1538-4357/ab4a11)
- Sakai, N., Nagayama, T., Nakanishi, H., et al. 2020, *PASJ*, 72, 53, doi: [10.1093/pasj/psz125](https://doi.org/10.1093/pasj/psz125)
- Sanna, A., Reid, M. J., Dame, T. M., et al. 2012, *ApJ*, 745, 82, doi: [10.1088/0004-637X/745/1/82](https://doi.org/10.1088/0004-637X/745/1/82)
- Steehhs, D., McClintock, J. E., Parsons, S. G., et al. 2013, *ApJ*, 768, 185, doi: [10.1088/0004-637X/768/2/185](https://doi.org/10.1088/0004-637X/768/2/185)
- Veledina, A., Muleri, F., Poutanen, J., et al. 2023, arXiv e-prints, arXiv:2303.01174, doi: [10.48550/arXiv.2303.01174](https://doi.org/10.48550/arXiv.2303.01174)
- Webster, B. L., & Murdin, P. 1972, *Nature*, 235, 37, doi: [10.1038/235037a0](https://doi.org/10.1038/235037a0)
- Wu, Y. W., Sato, M., Reid, M. J., et al. 2014, *A&A*, 566, A17, doi: [10.1051/0004-6361/201322765](https://doi.org/10.1051/0004-6361/201322765)